

VLBI OBSERVATIONS OF EXPANSION IN CYGNUS X-3

L. A. MOLNAR, M. J. REID, AND J. E. GRINDLAY

Harvard-Smithsonian Center for Astrophysics

Received 1987 November 12; accepted 1988 February 2

ABSTRACT

We have made VLBI observations at 1.3 cm wavelength of two flares in 1985 February. Fitting these data with simple dynamic models, we arrive at the following conclusions. The times at which flares began are consistent with our previously published period of 4.95 hr (significantly offset from the orbital period of 4.79 hr). The data are neither consistent with simple, static source structure nor simple, circularly symmetric structure. The data are consistent with a source expanding linearly in time from zero size at the flare beginning along a north-south axis (and possibly also expanding at a smaller rate along the transverse axis). This expanding structure is convolved with a fixed-size Gaussian (FWHM 0.68 ± 0.08 mas) consistent with an extrapolation of longer wavelength measurements of interstellar scattering. Interpreting the elongation as the bulk motion of a double-sided jet, we estimate the projected bulk velocity lies between $0.16c$ and $0.31c$ where both statistical and systematic effects are fully accounted for, a range that includes the actual bulk velocity of SS 433 ($0.26c$). We estimate the expansion transverse to the jet axis to be $0.13 \pm 0.02c$, in quantitative agreement with our previously predicted range of $0.05c$ to $0.25c$.

Subject headings: interferometry — radiation mechanisms — stars: individual (Cyg X-3) — stars: radio radiation — X-rays: binaries

I. INTRODUCTION

Since the first giant radio flare was observed in Cygnus X-3 in 1972 September, the light curves of giant flares have been interpreted in terms of an expanding cloud of synchrotron electrons (Gregory *et al.* 1972). Very Large Array (VLA) and Multiple Element Radio Linked Interferometer (MERLIN) observations made following giant flares in 1982 and 1983 gave the first indication that the radio source is elongated after a giant flare (Geldzahler *et al.* 1983; Spencer *et al.* 1986, and our observations discussed below). Observational similarities to extragalactic radio sources and other X-ray binaries (White and Holt 1982; Molnar 1985, 1986) suggest that the elongation could be indicative of an expanding jet, aligned with the rotation axis of an accretion disk. However, limited telescope resolution, the large amounts of interstellar scattering, and the temporal overlap of flares make it difficult to specify the source structure at one epoch and to track the evolution of that structure with time.

Our VLA observations of the spectral evolution of Cyg X-3 in its low radio state (Molnar, Reid, and Grindlay 1984, 1985) gave the first indication that the small-to-moderate flux density variations seen in the low state are simply smaller versions of the giant flares: expanding synchrotron sources in a jet. This paper describes very long baseline interferometric (VLBI) observations at 1.3 cm wavelength made in 1985 February that confirm this interpretation. In § II, we describe how the observations were made and calibrated. In § III, we analyze the data by fitting them to two simple, dynamic models, and discuss the implications of our results for the source structure. In § IV, we assess the potential for future observations.

II. THE OBSERVATIONS

a) Very Long Baseline Interferometry

We scheduled 6 hr observing runs on 1985 February 5 and 8, at 1.35 cm wavelength (detecting IEEE left circular polarization except at Effelsberg, which was detecting linear polarization) using MkIII recording terminals at five stations (Effelsberg [B], Haystack [K], Green Bank¹ [G], the VLA¹ [Y], and Owens Valley [O]). In designing the experiment, we chose the shortest wavelength available in order to have the best chance at studying an *isolated* flare. Molnar, Reid, and Grindlay (1984, 1985) found that flares are more luminous and briefer in duration at shorter wavelengths. Also, interstellar scattering (which depends on wavelength squared) sets a minimum size the flare must reach before it can be observed to expand.

As flare amplitudes vary over a wide range and cannot be predicted, we used the MkIII system in mode A to get the maximum recorded bandwidth of 56 MHz. Due to limited quantities of videotape we recorded only 10 6 minute scans on Cyg X-3 each day at intervals of about 35 minutes. The 6 minute scan lengths approximately matched the interferometer coherence limit set by atmospheric fluctuations. We used between 16 and 20 VLA antennas in phased mode for the added sensitivity, and we used the remaining antennas in a subarray to monitor the total flux density variations at other wavelengths during the experiment (§ IIb).

Our previous observations (Molnar, Reid, and Grindlay 1984, 1985) indicated the flares recur with a period of 4.95 hr. We considered a 6 hr run the minimum sufficient to make complete observations of one flare. Six hours is also the maximum duration of simultaneous visibility for the five stations. We scheduled two runs to improve our chances of getting good weather at all stations and a detectable flare on at least one run.

¹ Green Bank and the VLA are facilities of the National Radio Astronomy Observatory which is operated by Associated Universities, Inc., under contract with the National Science Foundation.

TABLE 1
EFFECTIVE SYSTEM TEMPERATURES (Jy)

| JD-2,446,100 | B | K | G | Y | O |
|--------------|------|-------|------|-------|-------------------|
| 2.0715..... | 68. | 1458. | ... | 1515. | 1466. |
| 2.0986..... | 66. | 1404. | ... | 1111. | 1259. |
| 2.1201..... | 66. | 1404. | ... | 1128. | 1158. |
| 2.1472..... | 68. | 1526. | ... | 1176. | 1044. |
| 2.1688..... | 69. | 1634. | ... | 1040. | 496. ^a |
| 2.1965..... | 79. | 1647. | ... | 1347. | 470. |
| 2.2174..... | 86. | 1512. | ... | 1132. | 484. |
| 2.2382..... | 97. | 1539. | ... | 1221. | 515. |
| 2.2590..... | 107. | 1566. | ... | 1307. | 580. |
| 2.2799..... | 127. | 1607. | ... | 1525. | 685. |
| 5.0715..... | ... | 986. | 545. | 578. | 763. |
| 5.0986..... | ... | 960. | 470. | 547. | 661. |
| 5.1201..... | ... | 973. | 427. | 559. | 599. |
| 5.1472..... | ... | 1037. | 396. | 578. | 513. |
| 5.1757..... | ... | 1088. | 371. | 590. | ... |
| 5.1965..... | ... | 1050. | 388. | 596. | ... |
| 5.2174..... | ... | 1050. | ... | 618. | ... |
| 5.2382..... | ... | 1050. | ... | 672. | ... |
| 5.2590..... | ... | 1024. | ... | 732. | ... |
| 5.2799..... | ... | 1037. | ... | 640. | ... |

^a Abrupt change reflects turning off front end beam switching.

The procedure for calibration of antenna gains is important, especially as 1.35 cm wavelength observations are particularly sensitive to antenna pointing errors and changing weather. Table 1 shows the effective system temperatures in janskys (after correction for various effects described below) that were applied to the data. These values were derived from the following procedure. Between Cyg X-3 scans, we made system temperature measurements and antenna temperature measurements on DR 21 (an 18.5 Jy, 20" diameter, H II region only 1.4 from Cyg X-3) with the "40 m" antennas (G, K, and O) and on 2005+403 (a 3.0 Jy extragalactic source 2.4 from Cyg X-3) with the "large" antennas (B and Y) to check the pointing and the gain. We also made two minute scans of 3C 345 each day to calibrate the relative phases of the 28 two-MHz tracks and to check the relative flux density calibration of the 40 m and the large antennas.

The VLA was in its largest configuration (A array). As it was unlikely that Cyg X-3 would be bright enough to use it to "phase the array," we phased on 2005+403, and offset the phase to compensate for the angular distance between the two sources. This angle must be known to within a fraction of the instantaneous synthesized beam of the array of about 0.08. We used observations made in 1983 December 3 (with the hybrid A/B array) to derive a position offset of Cyg X-3 from 2005+403: $\Delta\alpha(1950) 24^m 38^s 0563 \pm 0^s 0009$, $\Delta\delta(1950) 26^{\circ} 10' 926 \pm 0'' 010$. To further ensure that this positional error was unimportant, the outer two antennas on each arm were not used in the VLBI observation, increasing the instantaneous synthesized beamwidth to about 0.1. The signals of the antennas which were combined and recorded on the MkIII tapes were also passed through the normal VLA correlators. We calibrated the effective gain of the phased VLA with the standard VLA cross-correlations using the calibration formulation derived by Crane (1984).

No data were recorded at Green Bank on February 5 because the wrong epoch of precession was used to point the telescope. No data were recorded at Effelsberg on February 8 because of snow. No useful data were obtained at Owens Valley after 16 UT on February 8 because of rain.

For each measurement, the postcorrelation software searched a range of delays and fringe rates. In Table 2, we list the largest amplitude flux density found in each search, the rms of the values searched, and information on the baseline and time. The sizes of the search "windows" were narrowed when a specific prediction about the delay and rate could be made based on other detections either from the same baseline or on two other baselines that form a triangle with the baseline of interest. Even so, because of the large number of values searched for each detection the smallest signal-to-noise ratio (SNR) for a firm detection is about 6. There are 18 detections, one probable detection (marked with a "?"), and 18 interesting upper limits in Table 2.

b) Total Flux Density Light Curve

The VLA cross-correlations of the 1.3 cm data were used to derive a total flux density light curve. Those VLA antennas not used for the VLBI data were used to monitor the total flux density of Cyg X-3 at other wavelengths. On February 5, we used 16 inner antennas to observe alternately at 1.3 cm (22,235 MHz) for the VLBI recordings and at 2 cm (14,965 MHz) and 20 cm (1452 MHz) between VLBI scans; we used the seven outer antennas to monitor the total flux density at 6 cm (4885 MHz). The remaining four antennas were out of service. On February 8 we used 20 inner antennas to continuously track at 1.3 cm; we used seven outer antennas to monitor the total flux density alternately at 6 cm (4835 MHz and 4885 MHz, measured simultaneously using two independent pairs of intermediate frequency [IF] channels) and 18 cm (1652 MHz) and 20 cm (likewise measured simultaneously). The 1.3, 2, and 6 cm band observations had 50 MHz bandwidths, and the 18 and 20 cm band observations had narrower 25 MHz bandwidths to avoid interference problems.

Absolute flux density calibration was based on 3C 286 at 1.3 cm wavelength, on 1803+784 at 2 and 6 cm wavelengths, and on 2005+403 at 18 and 20 cm wavelengths. The 3C 286 and 1803+784 flux densities were used to establish the flux densities of

TABLE 2
CORRELATED FLUX DENSITIES

| Baseline | JD-2,446,100 | S_v (mJy) | σ_{S_v} (mJy) | u (fringes per arcsecond) | v (fringes per arcsecond) |
|----------|--------------|-------------|----------------------|-----------------------------|-----------------------------|
| BY | 2.0715 | <13. | 3. | 2774.3 | -24.2 |
| BY | 2.0986 | <14. | 4. | 2835.1 | 289.9 |
| BY | 2.1201 | <11. | 3. | 2824.7 | 541.6 |
| BY | 2.1472 | <19. | 4. | 2738.0 | 853.1 |
| BY | 2.1688 | <8. | 3. | 2612.1 | 1091.1 |
| BY | 2.1965 | <11. | 3. | 2379.3 | 1377.8 |
| BY | 2.2174 | <15. | 3. | 2156.5 | 1573.0 |
| BY | 2.2382 | <13. | 4. | 1896.6 | 1747.4 |
| BY | 2.2590 | <17. | 4. | 1604.0 | 1898.0 |
| KG | 5.0715 | 128. | 7. | 265.2 | 45.6 |
| KG | 5.0986 | 77. | 8. | 274.3 | 75.8 |
| KG | 5.1201 | 61. | 7. | 275.9 | 100.3 |
| KG | 5.1472 | 39. | 8. | 270.8 | 130.9 |
| KG | 5.1757 | ?29. | 6. | 259.9 | 162.0 |
| KG | 5.1965 | <25. | 6. | 241.5 | 183.4 |
| KY | 2.0715 | <79. | 17. | 788.0 | -330.2 |
| KY | 2.0986 | <98. | 20. | 914.5 | -234.8 |
| KY | 2.1201 | <64. | 13. | 996.2 | -149.9 |
| KY | 2.1472 | <90. | 20. | 1072.9 | -34.0 |
| KY | 2.1688 | <71. | 14. | 1111.7 | 63.2 |
| KY | 5.0715 | <33. | 8. | 828.9 | -302.8 |
| GY | 5.0715 | 36. | 6. | 563.7 | -348.4 |
| OG | 5.0715 | <23. | 6. | -573.0 | 657.4 |
| OY | 2.0715 | 163. | 15. | 9.0 | 308.9 |
| OY | 2.0986 | 126. | 17. | -51.3 | 306.5 |
| OY | 2.1201 | 229. | 11. | -98.2 | 299.9 |
| OY | 2.1472 | 373. | 17. | -154.8 | 285.7 |
| OY | 2.1688 | 539. | 8. | -196.3 | 270.1 |
| OY | 2.1965 | 345. | 8. | -244.6 | 244.8 |
| OY | 2.2174 | 262. | 7. | -276.0 | 222.4 |
| OY | 2.2382 | 171. | 8. | -302.7 | 197.5 |
| OY | 2.2590 | 116. | 9. | -324.2 | 170.5 |
| OY | 2.2799 | 147. | 11. | -340.1 | 141.9 |
| OY | 5.0715 | 73. | 7. | -9.3 | 308.9 |
| OY | 5.0986 | 51. | 8. | -69.3 | 304.5 |
| OY | 5.1201 | 41. | 6. | -115.6 | 296.3 |
| OY | 5.1472 | <29. | 7. | -170.8 | 280.2 |

2005+403 and 3C 345 at the shorter wavelengths, which were assumed to be constant over the observing run. The assumed and derived flux densities are listed in Table 3. The uncertainty in the absolute flux density calibration is dominated by the uncertainty in the values of the references, which is less than 20% at 1.3 cm wavelength, and less than 10% at the longer wavelengths.

The source 2005+403 was observed within 15 minutes of each Cyg X-3 scan at 1.3 cm wavelength and within 30 minutes of each scan at 6, 18, and 20 cm wavelength. These 2005+403 observations were used to calibrate the antenna-gain amplitudes for the Cyg X-3 observations. The phases were "self-calibrated": calibrated with the Cyg X-3 data under the reasonable assumption that the structure of Cyg X-3 made no contribution to the phase. (This assumption is justified for elliptical Gaussian structure.) Flux densities and uncertainties were then computed by averaging the real parts of the calibrated complex visibilities. Before averaging, a

TABLE 3
CALIBRATIONS CONSTANTS

| Source | λ (cm) | S_v (Jy) | (u, v) restrictions |
|----------------|------------------|--------------------|----------------------------|
| 3C 286 | 1.3 ^a | 2.55 | inner two antennas per arm |
| 3C 345 | 1.3 | 11.6 | |
| 1803+784 | 1.3 | 3.72 (0.08) | |
| | 2 | 3.331 ^a | |
| | 6 | 2.5 ^a | |
| | 20 | 1.674 (0.003) | |
| 2005+403 | 1.3 | 3.00 | |
| | 2 | 2.93 | |
| | 6 | 4.262 (0.011) | |
| | 18 | 4.027 ^a | |
| | 20 | 4.000 ^a | |

^a Assumed values.

correction was made for scattering using the scattering law of Wilkinson, Spencer, and Nelson (1987), an increase of between 3% and 8% for the 18 and 20 cm wavelength data on February 8. Baselines shorter than 20,000 ns were not used at 18 and 20 cm to avoid confusion from large angular scale sources in or near the primary beam of each 25 m antenna.

Figures 1 and 2 show the flux density of Cyg X-3 versus time on the two days. These light curves are qualitatively similar to our earlier observations (Molnar, Reid, and Grindlay 1984, 1985): they show a series of overlapping flares each of which evolves spectrally with time from optically thick (flux density decreasing with wavelength) to thin (flux density increasing with wavelength). We describe here the timing of the flares as determined by the light curves for use in the next section.

The light curve of February 5 is generally dominated by a flare that peaks near JD 2,446,102.17 at 1.3 cm wavelength. Near the beginning of the observing there is additional structure (a brief increase and decrease) that may be interpreted as substructure of the main flare or as a separate flare. It is of small enough amplitude not to affect the VLBI visibilities significantly. It increases slightly the uncertainty of when the main flare began, which we estimate to have been at JD 2,446,102.05 \pm 0.03. At the end of the observation we see the beginning of the next flare at JD 2,446,102.26 \pm 0.01 at 1.3 cm wavelength.

The negative spectral index (α , where $S_\nu \propto \nu^\alpha$) throughout the February 8 data set indicates the flux density has a significant contribution from the decaying flux density of a large flare that peaked before we began observing. Superposed on this is a small flare that is still rising at the beginning of the observation, and that peaks around JD 2,446,105.06. Also superposed is a very small flare that begins at JD 2,446,105.150 \pm 0.002.

The optically thin spectrum is consistently found to approach asymptotically a power law with spectral index ~ -0.5 (e.g., 1972 September, Gregory and Seaquist 1974; 1983 September 17, Molnar, Reid, and Grindlay 1984). This is seen, for example, in our data from late on 1985 February 8, shown in Figure 3, at which time all flares contributing to the flux density were optically thin.

We describe the large flare on February 5 as an isolated flare in that, at least following its peak, the large majority of the total 1.3 cm flux density seems to come from that flare. In contrast the total flux density on February 8 seems to be dominated by a flare (or flares) that began sometime between February 5 and 8. As our hypothesis is that each flare is an expanding source, we can check the consistency of our interpretation of the light curve by looking for evidence in the VLA data alone that the source is extended, which we would expect to be the case on February 8, but not on February 5. As a test, we divided the visibilities at 1.3 and 6 cm from February 8 by the light curve and fitted an elliptical Gaussian to all the data from each wavelength. The best fit to the 1.3 cm data

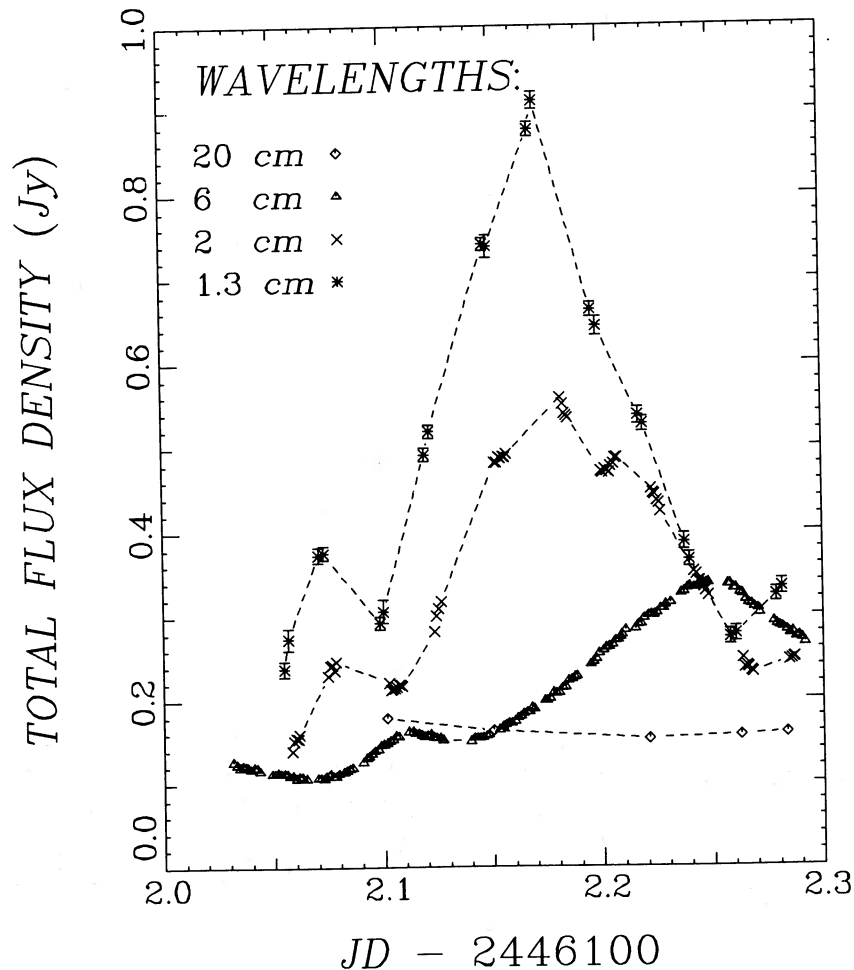


FIG. 1.—Total flux density vs. time on 1985 February 5 measured at the VLA

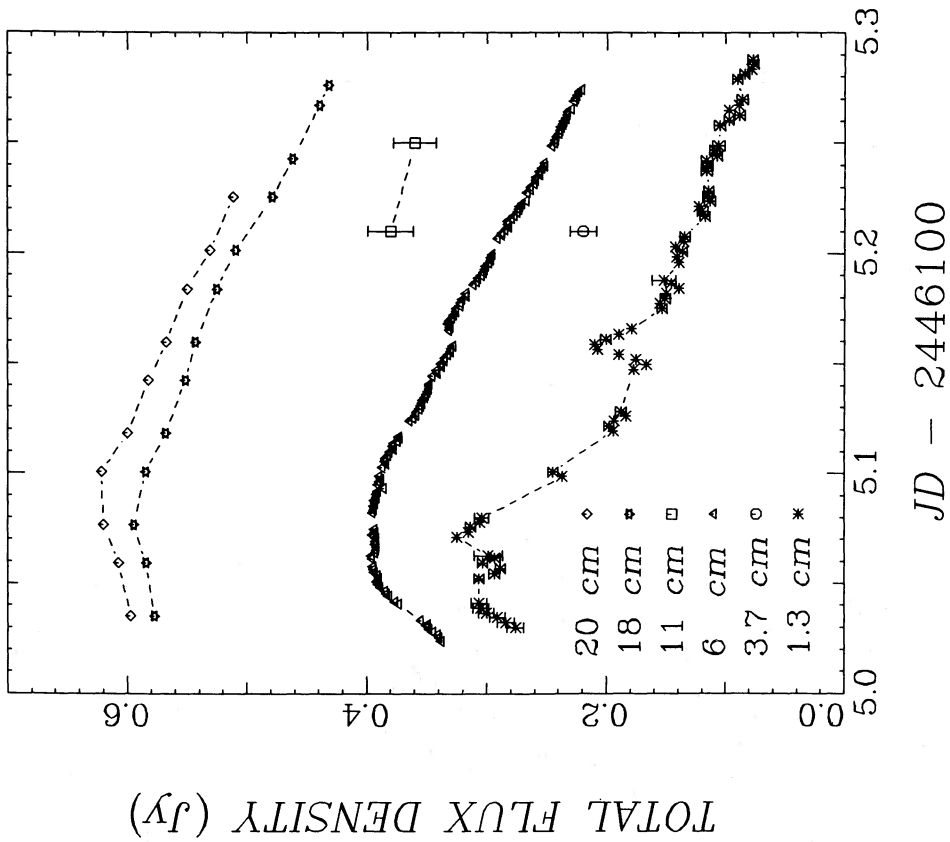


FIG. 2

FIG. 2.—Total flux density versus time on 1985 February 8. The 3.7 and 11 cm values are from the three-element interferometer at Green Bank, West Virginia (K. Johnston, private communication); all other values are from the VLA.

FIG. 3.—Total flux density of Cyg X-3 vs. frequency at JD 2,446,102.17 and at JD 2,446,105.21. The 8.1 and 2.7 GHz values are from the three-element interferometer at Green Bank, West Virginia (K. Johnston, private communication); all other values are from the VLA.

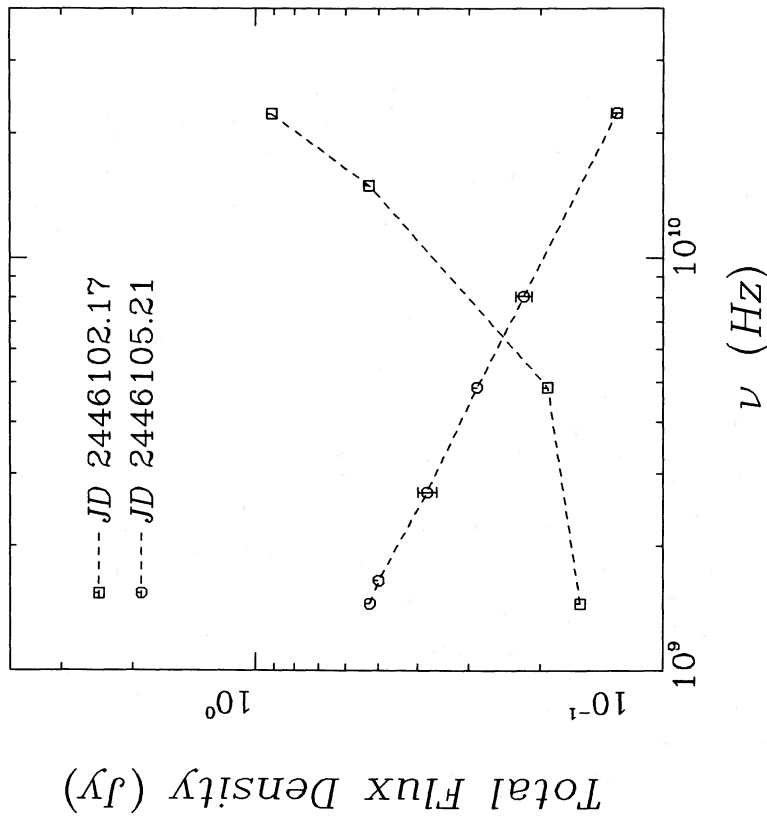


FIG. 3

has a major axis, minor axis, and a position angle measured east of north (θ_M, θ_m, χ) of (19 ± 2 mas, < 10 mas, $-8^\circ \pm 10^\circ$). The best fit to the 6 cm data is (30 ± 2 mas, 24 ± 2 mas, $11^\circ \pm 12^\circ$). Both data sets show significant evidence of an extended component. The difference in size at the two wavelengths is likely due to greater scattering at 6 cm and a larger fractional contribution by the new, unresolved flare at 1.3 cm.

Analysis of the VLA visibilities indicates no linear polarization in the emission of Cyg X-3 with upper limits of 2% at 2 cm, 0.4% at 6 cm, and 1% at 20 cm wavelength. We place an upper limit on circular polarization at these wavelengths at a few percent.

III. THE ANALYSIS

In this section we investigate what can be learned about the structure of Cyg X-3 from our VLBI data. The large amplitude variations of flux density on the time scale of hours (Figs. 1 and 2) imply significant changes in the source structure on that time scale. In principle one should make an independent map for each integration time to resolve the changing structure. However, the data at any one integration time are insufficient to do this. We therefore fit the data to a time-dependent model that is sufficiently general to answer our basic questions about the evolution of the source structure. In the following subsections we (a) describe the model we have chosen to fit the data; (b) discuss those model parameters which are fixed by information external to the VLBI data set; (c) present the fit of the VLBI data to the model; and (d) interpret the astrophysical implications of the model.

a) Model: Expanding Elliptical Gaussian with Scattering

We model a single flare as an elliptical Gaussian of fixed axial ratio, A , and orientation, χ (measured positive east of north), with the full width at half-maximum (FWHM) of the major axis expanding at a constant rate, $\dot{\theta}_M$, with time, t , from zero size at flare onset, and convolved with a circular Gaussian scattering disk of FWHM θ_{scat} . We further take the flares to recur with a period, P . Given a reference flare with onset at time t_0 , we may describe the time of onset of the flare n cycles later as $t_n = t_0 + nP$. As the convolution of two Gaussians is itself a Gaussian, we may describe the n th flare as an elliptical Gaussian with FWHM of the major axis

$$\theta_{M_{\text{obs}}}^2(t) = \theta_{\text{scat}}^2 + [\dot{\theta}_M(t - t_0 + nP)]^2 \quad (1)$$

oriented at an angle χ , and with FWHM of the minor axis

$$\theta_{m_{\text{obs}}}(t) = \theta_{\text{scat}} + \left[\frac{\dot{\theta}_M}{A} (t - t_0 + nP) \right]^2. \quad (2)$$

The correlated flux density for an interferometer with east and north projections as seen by the source measured in wavelengths of u and v , respectively, for an elliptical Gaussian described by $(\theta_{M_{\text{obs}}}, \theta_{m_{\text{obs}}}, \chi)$ is

$$V(u, v) = S \exp \left\{ -\frac{\pi^2}{4 \ln 2} [\theta_{M_{\text{obs}}}^2 (u \sin \chi + v \cos \chi)^2 + \theta_{m_{\text{obs}}}^2 (u \cos \chi - v \sin \chi)^2] \right\}, \quad (3)$$

where S is the total flux density of the flare.

This model allows in a simple manner for the following elements of source structure: expansion in one or two dimensions ($\dot{\theta}_M$ and A), interstellar scattering (θ_{scat}), and periodicity (P). (Operationally one-dimensional expansion refers to obtaining an observational upper limit on expansion along the transverse axis, as revealed by a lower limit on the model parameter A .) Below we give theoretical and observational reasons why these elements are necessary and sufficient for this analysis.

i) One-dimensional Expansion

Expansion in one dimension might be expected by analogy with the radio emission of SS 433, which has a twin jet morphology (Abell and Margon 1979; Hjellming and Johnston 1981a, b). Like SS 433, Cyg X-3 is an X-ray binary source with an accretion disk and an accretion disk corona (White and Holt 1982; Molnar 1985; Molnar and Mauche 1986). The normal to the disk plane is a natural preferred jet axis; this subject has been pursued theoretically by many authors (e.g., Ferrari *et al.* 1985).

Observations of several giant flares with the VLA and with MERLIN have shown Cyg X-3 to become detectably elongated several weeks after a giant flare. (The resolution of these data is generally insufficient to determine if the source also became extended along its minor axis.) Geldzahler *et al.* (1983) reported that, one month following the 1982 September giant flare, Cyg X-3 was elongated by a few tenths of an arcsecond along a north-south axis. Spencer *et al.* (1986) modeled data taken 1983 October 13, following several giant flares in early October, as a double separated by $0''.07$ along a north-south axis. An elliptical Gaussian fit to 20 cm VLA data we took on 1983 December 3-4, has best-fit parameters $(\theta_M, \theta_m, \chi)$ of $(292 \pm 7$ mas, 225 ± 11 mas, $4^\circ \pm 5^\circ$). The size of the minor axis is consistent with interstellar scattering (see below), but the major axis is significantly elongated, possibly from the 1983 October flares. Finally, the previous section describes elongation in our VLA data for 1985 February 8.

We note as an aside that, while all measurements of the position angle of the radio elongation (noted in this subsection and above in § IIIa) are consistent with a constant value $\sim 5^\circ$, they differ from the orientation ($\sim 40^\circ$) of the X-ray “wings” recently reported by Kifune *et al.* (1987). As the orientation of these wings is approximately parallel to the galactic plane, and as they show a good spatial correlation with extended radio sources in the Cygnus X region (DR 17, 21, and 22 on the east, and DR 4, 5, and 6 on the west), we suggest the X-ray “wings” are physically associated with these features (cf. the radio maps of Wendker [1970] or Downes and Rinehart [1966]). As these radio source are generally thought to be in a galactic arm only 2 kpc distant, we suggest that the X-ray wings are unrelated to Cyg X-3.

ii) Two-dimensional Expansion

The primary purpose of this experiment was to test our prediction (Molnar, Reid, and Grindlay 1984, 1985) that each flare in Cyg X-3, small or large, is a synchrotron source whose spectral evolution is dominated by adiabatic expansion in three dimensions. By

assuming the energy in the radio flares (i.e., in the particles and the magnetic field) is not much greater than that emitted as X-rays, we predicted a specific range of expansion velocity: $0.05c$ to $0.25c$. This should be observable as two-dimensional expansion in the plane of the sky. Our work was based on analysis of the spectral evolution of small to moderate size flares. This evolution is qualitatively similar to that seen in giant flare, which has long been interpreted as due to source expansion. Upper limits on VLBI visibilities measured on an east-west baseline during the 1972 September, giant flare are direct evidence that the source became extended transverse to its usual elongation axis during that flare (Hinteregger *et al.* 1972).

iii) *Interstellar Scattering*

Anderson *et al.* (1972) first suggested that some observed source structure in Cyg X-3 may be due to scattering in the interstellar medium (ISM). They measured a source diameter of $\sim 2''$ at 73 cm wavelength which they attributed to scattering. Wilkinson, Spencer, and Nelson (1987) reanalyzed the data of Anderson *et al.* and found a size of $2''.7 \pm 0''.3$. They also present MERLIN data at the same wavelength with which they find a size of $2''.8 \pm 0''.1$. The detailed dependence of fringe visibility on baseline length in these data suggests size should depend on wavelength to the 2.08 ± 0.03 power. We found no evidence of elongation in our 20 cm VLA data obtained on 1985 February 8, and fitted a circular Gaussian size of 229 ± 5 mas, consistent with the MERLIN size and scaling and with the size of the minor axis of the 1983 December data noted above. The 20 cm size measured on February 8 remained constant throughout the day despite the $\sim 30\%$ decrease in the total flux density. The difference between the 20 cm wavelength size and the 1.3 and 6 cm sizes (noted in § IIb) and the rapid variation of the 20 cm flux density are strong evidences that the observed 20 cm size (≥ 10 light days) is not intrinsic to the source. The MERLIN data predict a scattering size of 0.68 ± 0.09 mas at the wavelength of our VLBI measurements.

iv) *Periodicity*

We suggested the presence of a period in the radio data in Molnar, Reid, and Grindlay (1984), and derived a value for the period of 4.95 ± 0.04 hr in Molnar, Reid, and Grindlay (1985). We may therefore specify all times of flare onset given the time of onset for a single flare and the period between flares. Further evidence for this period and a detailed discussion of its physical implications will be presented elsewhere (Molnar *et al.* 1988). The physical origin of this period is unimportant for the present analysis. Here we need only establish that the period used suffices to describe the times of flare onset for those flares included in the VLBI analysis.

v) *Sufficiency*

The arguments above motivate the elements of expansion, elongation, scattering, and periodicity in our model. We need also to argue that it is sufficient to use a single parameter for each one of these things, and that we have not omitted any other important elements in the model. As a general argument, we note that as the expected scattering size at the wavelength of the VLBI data is within a factor of 2 of the expected intrinsic size reached in ~ 5 hrs the scattering would tend to obscure more detailed intrinsic structure. Also the data are of insufficient quality and quantity to distinguish very fine details, as we will demonstrate below by showing that the data can be well fitted to the model.

While the model equation (eq [3]) includes the total flux density, S , which is a function of time, information about the variation of source structure can be separated from that about the variation of the total flux density. Specifically, the total flux density cancels out of *ratios* of correlated flux densities. To restrict our analysis in this paper to structure evolution, we will work solely with ratios of flux densities.

Our model equation implicitly uses the size of the most recent flare; that is, it assumes this flare may be treated as isolated from previous flares. Given the limited range of baseline lengths and the large expansion velocities expected, the VLBI correlated flux densities are likely to be sensitive to only one flare at a time because of the large difference in spatial size between the flare in progress (a few hours old) and the previous flares (more than 6 hr old). Hence we may include in our analysis all ratios of VLBI correlated flux density, both detections (3 OY/KG ratios and 1 GY/KG ratio on February 8) and upper limits (9 BY/OY and 5 KY/OY ratios on February 5 and one each of OG/KG, KY/KG, and OY/KG ratios on February 8). For scans with only one VLBI detection, we may consider the ratio of the VLBI correlated flux density to the total flux density (S , at "zero length" baseline), but only when the most recent flare dominates. From the description of the light curve in § IIb we see this is only true on February 5 approximately from the flare peak to its subsequent trough (5 OY/ S ratios). In all we have nine ratios of detections and 17 usable ratios of upper limits to detections to which we can fit our model.

We have six model parameters. In the next subsection (§ IIIb) we fix one parameter, χ , using the VLA structure information discussed in § IIb, and two other parameters, t_0 and P , using the VLA light curve. In § IIIc we will use the VLBI data to determine the remaining parameters: θ_M , A , and θ_{scat} .

b) *Parameters Fixed by the VLA Data: χ , t_0 , and P*

For our model fit, we take an orientation of the major axis, $\chi = 5^\circ$, consistent both with the elliptical Gaussian fits to the VLA data of February 8 in § IIb and the orientations measured at other times for giant flares (noted in § IIIa). We also take the time of flare onset, $t_0 = \text{JD } 2,446,102.05 \pm 0.03$, measured in § IIb from the light curve for the large flare on February 5. Finally, we take the period, $P = 4.95 \pm 0.04$ hr, given in Molnar, Reid, and Grindlay (1985). As noted above, we need only to establish that this period gives a sufficient description of the times of flare onset for those flares with detectable VLBI fringes: the large flare on February 5 and the flare in progress at the beginning of February 8.

As a general check on whether the radio period is applicable during these observations, we consider the three times of flare onset estimated directly from the light curve: two on February 5, and one midway into the February 8 observation. The period quoted above implies the time between the February 5 flares is 1.02 ± 0.15 cycles and that between the first flare on February 5 and the flare on February 8 is 15.03 ± 0.19 cycles. (The uncertainties in these values are dominated by uncertainties in flare timing rather than uncertainty in the radio period.) The probability of both of these differences falling within the given errors of an integer by random

chance is 9%. (This is computed from the binomial distribution assuming two successes in two independent trials each with a 30% random chance of success.) We conclude the flare timing during our observations was consistent with the period given in Molnar, Reid, and Grindlay (1985) and marginally inconsistent with random timing.

A direct check on the timing of the first February 8 flare can be made from the VLBI data by estimating the source size at a given time during that flare and determining at what time the February 5 flare was the same size. Specifically, the single scan with the most detections is at JD 2,446,105.0715, for which we have three detections, two upper limits, and the total flux density. The three detections are enough to determine the parameters of an elliptical Gaussian with major axis oriented at 5° : $(S_{\text{com}}, \theta_M, \theta_m)$ is $(154 \pm 11 \text{ mJy}, 1.49 \pm 0.11 \text{ mas}, 0.78 \pm 0.10 \text{ mas})$, where S_{com} is the flux density of the compact flare component, not the total flux density. This solution is consistent with the observed total flux density and the upper limits on correlated flux density. (Note that solutions that do not violate these additional restrictions exist only in the range of position angles $[-3^\circ < \chi < 34^\circ]$, a further confirmation of our choice of position angle)

In Figure 4 we show the measured OY visibilities when the large flare dominated the February 5 flux density and compare them with model visibilities based on the static elliptical Gaussian determined above. The model visibility rises with time because the projected baseline orientation is swinging from north-south (the orientation of the major axis) toward east-west. In contrast the measured visibilities decrease by 30%. We note that for a fixed size circular Gaussian, the visibility would be expected to decrease 10%, due to the 10% increase in baseline length. Hence assuming only that the source is elongated north-south the decrease in visibility is direct evidence that the source size is rapidly increasing with time. Assuming the February 5 and 8 flares had the same structural evolution, the point where the two functions cross, JD 24,46,102.183 \pm 0.002, marks the time when the February 5 flare was the same size as the February 8 flare was at JD 2,446,105.0715. These two times differ by 14.00 ± 0.01 cycles of the radio period, indicating the radio period does reliably fix the time of flare onset for the February 8 flare.

c) Fitting the VLBI Data

In § IIIb we determined *a priori* values for three of the model parameters: $(\chi, t_0, P) = (5^\circ, \text{JD } 2,446,102.05, 4.95 \text{ hr})$. This leaves three parameters, θ_M , A , and θ_{scat} , to be determined by nine ratios of VLBI correlations and 17 limits on ratios. Specifically, we want

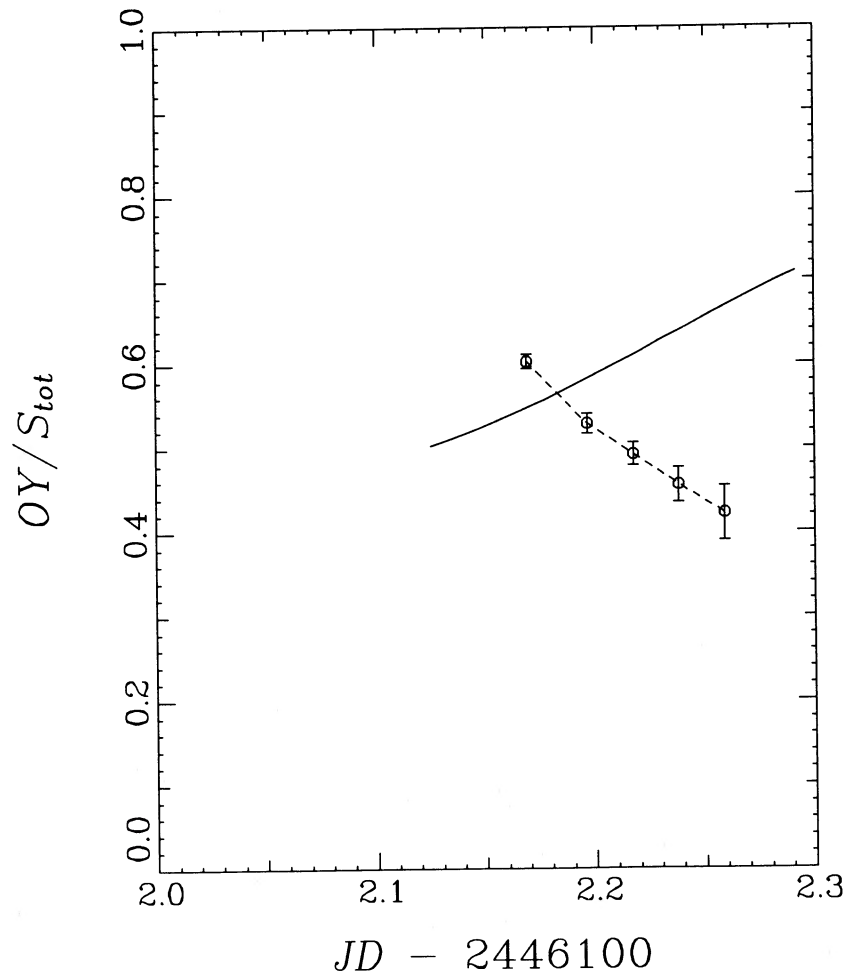


FIG. 4.—Ratio of OY correlated flux density to the total flux density as a function of time on 1985 February 5. The solid curve is the prediction of the static elliptical Gaussian model for February 8.

to determine the best-fit model parameters and check that they provide a good fit to the data, as well as to estimate the statistical uncertainty of these parameters.

We will answer the statistical questions using a generalization of the χ^2 statistic developed in Avni (1976), Avni *et al.* (1980), and Avni and Tananbaum (1986). In order to use a given data set to make the strongest statement possible about a given scientific question, Avni (1976) distinguishes between interesting and uninteresting parameters. The increment in the statistic for a given confidence level depends on the number of interesting parameters, i.e., the number of parameters being estimated simultaneously, which may be less than the total number of parameters. For our model the number of interesting parameters is two (θ_M and A) when asking about the intrinsic structure of Cyg X-3, and one (θ_{scat}) when asking about the effect of the interstellar medium. Avni *et al.* (1980) extend the formalism generally to include measurements of upper limits, while Avni and Tananbaum (1986) specifically treat the case of upper limits with Gaussian distributed residuals. In this extension the information is lost as to whether the fit to the data is good, but no information is lost about confidence levels for the parameters given that one already has reason to trust the fit.

For points on a 3-dimensional grid in parameter space we compute the statistic

$$S(\theta_M, A, \theta_{\text{scat}}) = \sum_{i=1}^9 \left(\frac{R_i - R_{i\text{mod}}}{\sigma_{R_i}} \right)^2 - 2 \sum_{j=1}^{17} \ln \left[\frac{1}{2} \operatorname{erfc} \left(\frac{R_{j\text{mod}} - R_j}{\sqrt{2} \sigma_{R_j}} \right) \right], \quad (4)$$

where the first term on the right-hand side of the equation (index i) is a summation over the detections and the second term (index j) is a summation over the upper limits. R_i and R_j are the measured values σ_{R_i} and σ_{R_j} are their uncertainties, and $R_{\text{mod}}(i)$ and $R_{\text{mod}}(j)$ are the model ratios for a given parameter set, respectively. The smallest value of S , 3.94, was obtained for $(\theta_M, A, \theta_{\text{scat}})$ equal to $(0.40 \text{ mas h}^{-1}, 2.16, 0.68 \text{ mas})$. While S may not be used directly to test goodness of fit, we note that with the best-fit parameters none of the measured upper limits are less than the corresponding model values. Hence at this point we can compute a χ^2 by setting the second term in the equation above to zero (i.e., ignoring the upper limits.) We obtain a χ^2 of 3.10 with 6 degrees of freedom, which has a fractional probability of 0.80 of being exceeded when the model is correct, indicating a good fit to the data.

We show the fit to the measured visibility ratios graphically in Figures 5 and 6. In Figure 5 we show all of the February 5 OY

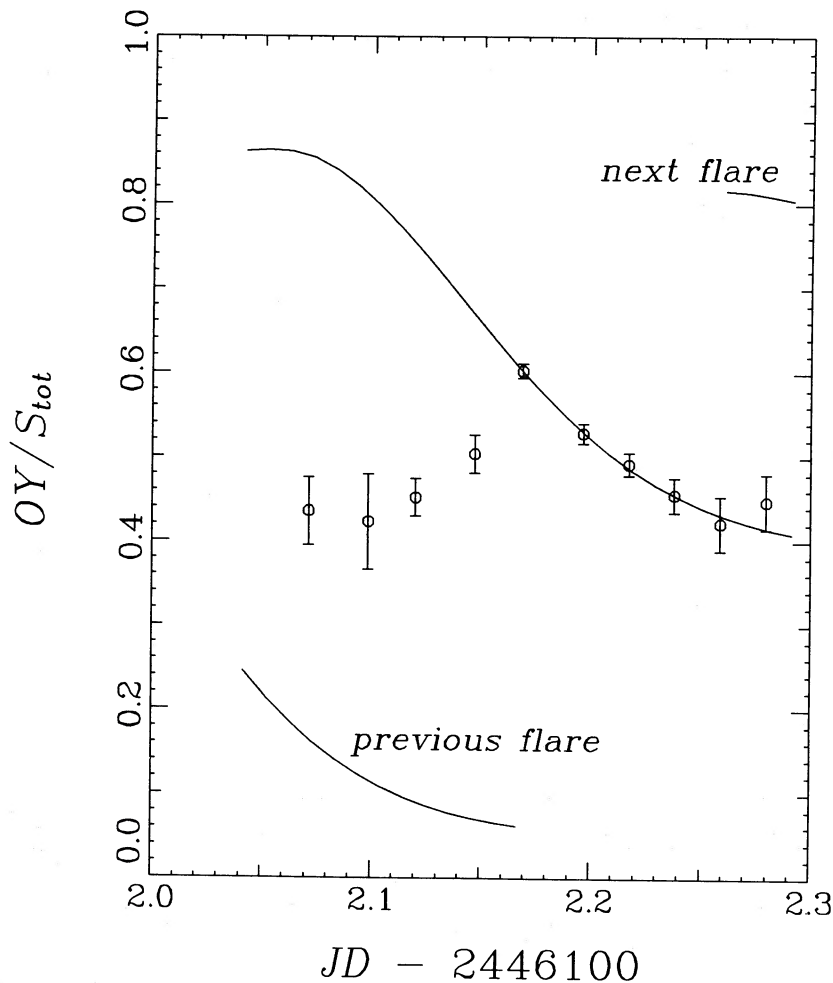


FIG. 5.—Ratio of OY correlated flux density to the total flux density as a function of time on 1985 February 5. The curves are the predictions of the expanding elliptical Gaussian model described in the text for each of three successive flares. Each model curve is plotted only for the range in which there was significant flux density contributed by the corresponding flare. Where two flares overlap, the observed data should fall between the model curves.

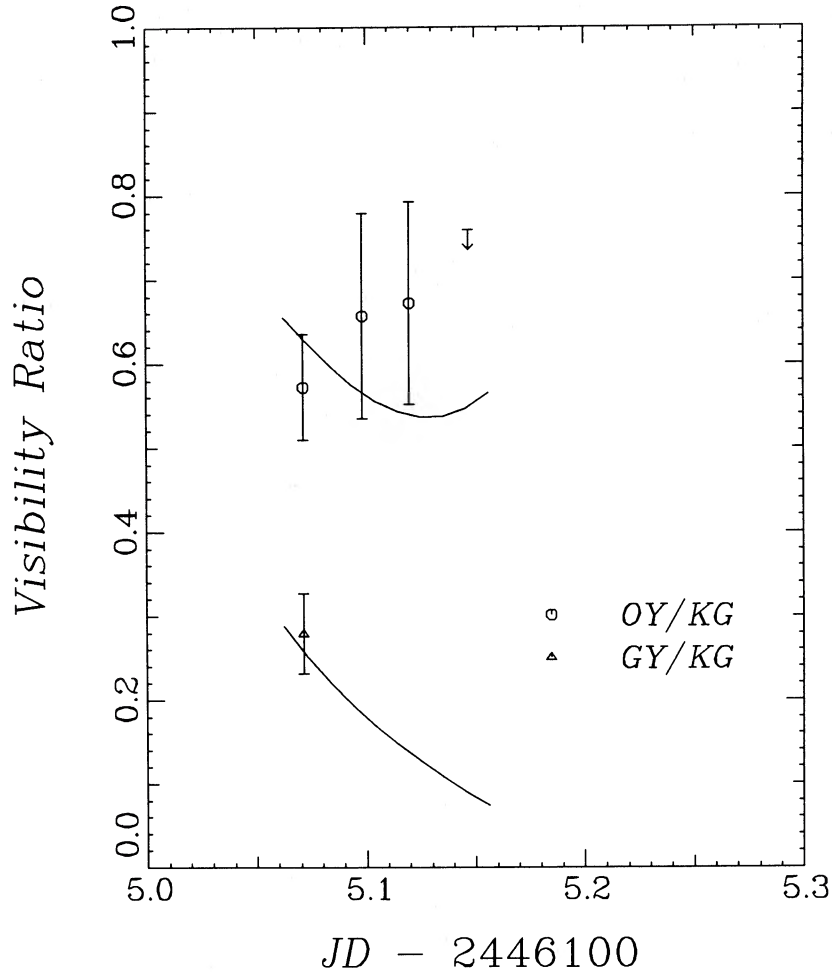


FIG. 6.—Ratios of correlated flux densities as a function of time on 1985 February 8 for OY/KG (circles and upper limit) and GY/KG (triangle). The curves are the predictions of the expanding elliptical Gaussian model described in the text.

visibilities, and model visibilities for the main flare as well as for identical preceding and following flares. Early on February 5, when the total flux density has comparable contributions from two flares, the data fall between the two model curves. Later, when just one flare dominates the total flux density, the data follow the model curve closely. At the very end, when a new flare begins to make a significant contribution, the measured value again lies between the two model curves. The data on February 8, shown in Figure 6, are all dominated by one flare and follow the model curves closely.

To show the expansion more directly, we take the orientation, intrinsic axial ratio, and scattering size determined from the model and use each of the OY visibilities from February 5 to determine the intrinsic FWHM of the major axis as a function of time (Fig. 7) For comparison we also plot the model size for the large flare of February 5, and the preceding and following flares (as in Fig. 5). As before, when the large flare dominates, the data fall on the model curve, and when two flares each have significant flux density the data fall between the two associated model curves.

In Figure 8 we show contour maps of how the model predicts that a single flare would appear at flare onset, and 1.7, 3.3, and 5.0 hr later. We show maps both with and without the interstellar scattering to illustrate at what point in the evolution of a flare the intrinsic length and width begin to affect the observed length and width.

In Figure 9 we plot our best value and 1σ through 5σ contours of the statistical uncertainty on the (A, θ_M) plane (considering θ_{scat} uninteresting and allowing it to vary). By 1σ contour, for example, we mean the intrinsic value lies within the contour at a 68% confidence level. Notice that the size of a 1σ variation depends strongly on direction in the plane. Taking θ_{scat} to be the only interesting parameter, its 1σ error is 0.08 mas. The excellent agreement of the measured scattering size with the predicted value based on the MERLIN data cited in § IIIa provides a good, though partial, confirmation of the model.

We recomputed the fit for other values of (χ, t_0, P) that were within the accuracy to which these parameters could be computed *a priori* to see how sensitive our fit was to these uncertainties. In Figure 10 we plot the best value and 1σ through 5σ probability contours for $(\chi, t_0, P) = (-5^\circ, \text{JD } 2,446,102.08, 4.95 \text{ hr})$, the case which shows the most extreme change from our original fit. Here the limits on the expansion velocity and the lower limit on the axial ratio are little changed, but where there had been a strict upper limit on the axial ratio now there is none. The fitted scattering size is now 0.83 ± 0.06 which is formally 2σ higher than previously. Again for the best-fit parameters, none of the measured upper limits are less than the corresponding model values. We obtain a χ^2 of

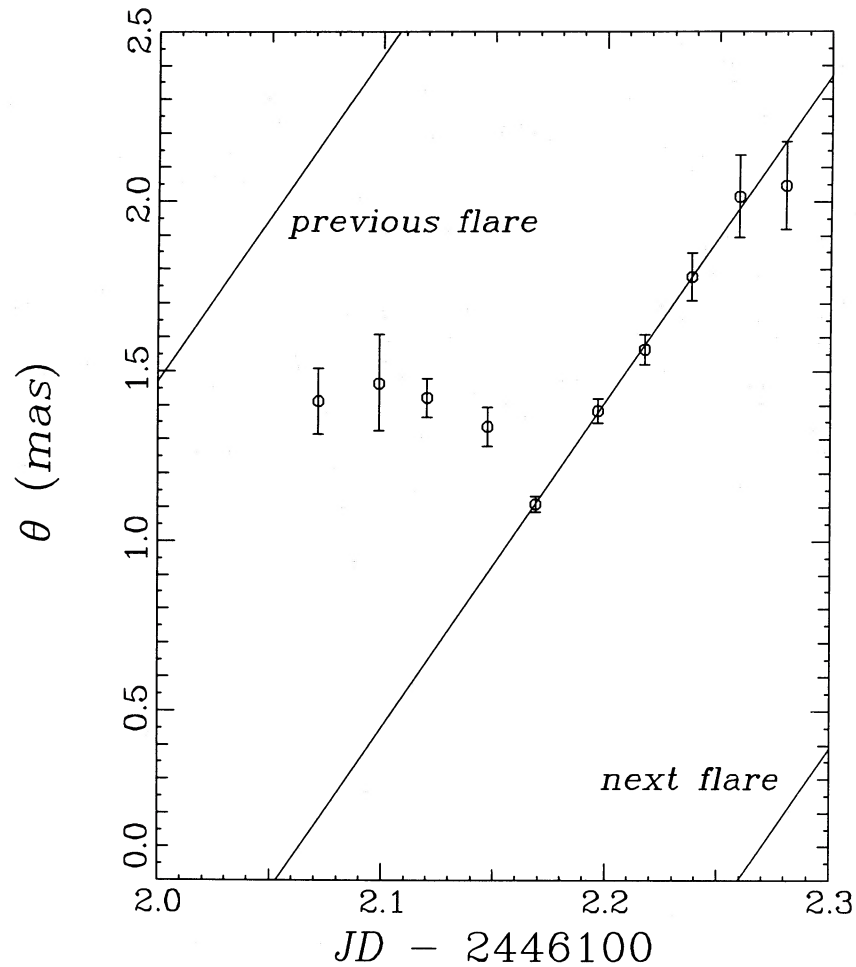


FIG. 7.—Observed FWHM of the major axis vs. time for the OY baseline on February 5. This is computed assuming an elliptical Gaussian with fixed orientation and intrinsic axial ratio, that is convolved with a fixed scattering size with parameters $(\theta_{\text{scat}}, \chi, A) = (0.68 \text{ mas}, 5^\circ, 2.16)$. Line represent best-fit linearly expanding, periodic model to all the data with parameters $(P, \theta_M, t_0) = (4.95 \text{ h}, 0.40 \text{ mas h}^{-1}, \text{JD } 2,446,102.05)$.

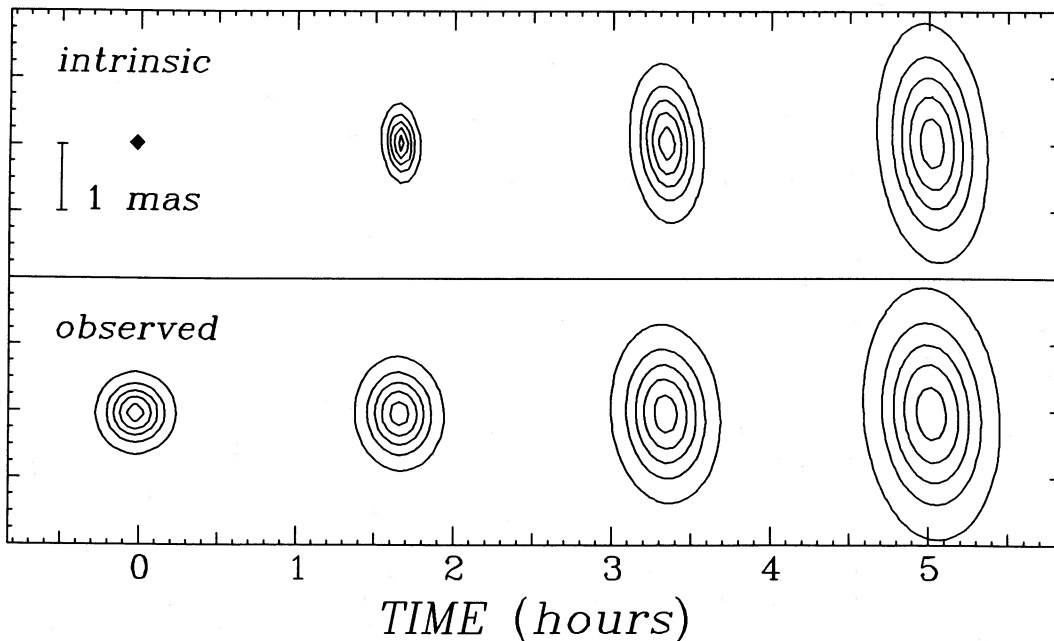


FIG. 8.—Contour maps of an expanding elliptical Gaussian model flare at flare onset, and 1.7, 3.3, and 5.0 hr later, using model parameters determined by the VLBI data. North is up and east to the left. A bar indicates the scale in milliarseconds. The map centers are offset horizontally according to the time they represent (as indicated on the x-axis). The upper row of maps represent the intrinsic source structure, while the lower row represent the observed source structure after inclusion of the effect of interstellar scattering. Contours are at 10%, 30%, 50%, 70% and 90% of peak brightness.

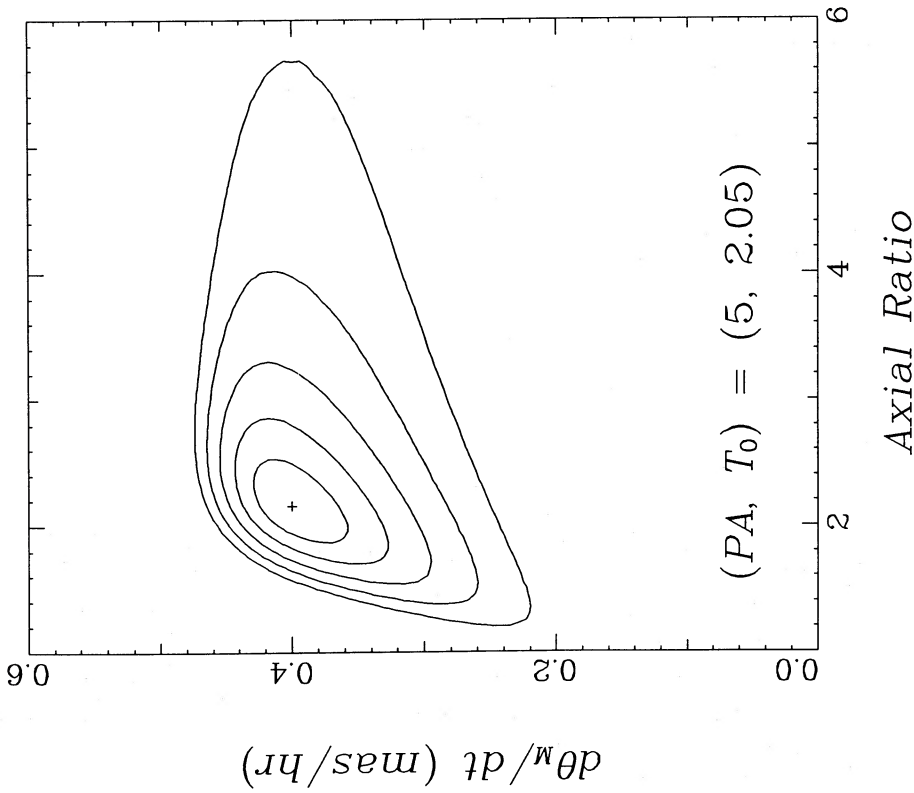


FIG. 9

FIG. 9.—The parameters θ_M vs. A of the expanding elliptical Gaussian model for the best set of *a priori* parameter values: $(\lambda, t_0, P) = (5^\circ, \text{JD } 2,446,102.05, 4.95 \text{ hr})$. A cross marks the best-fit values. Solid curves denote 1 σ through 5 σ error contours.

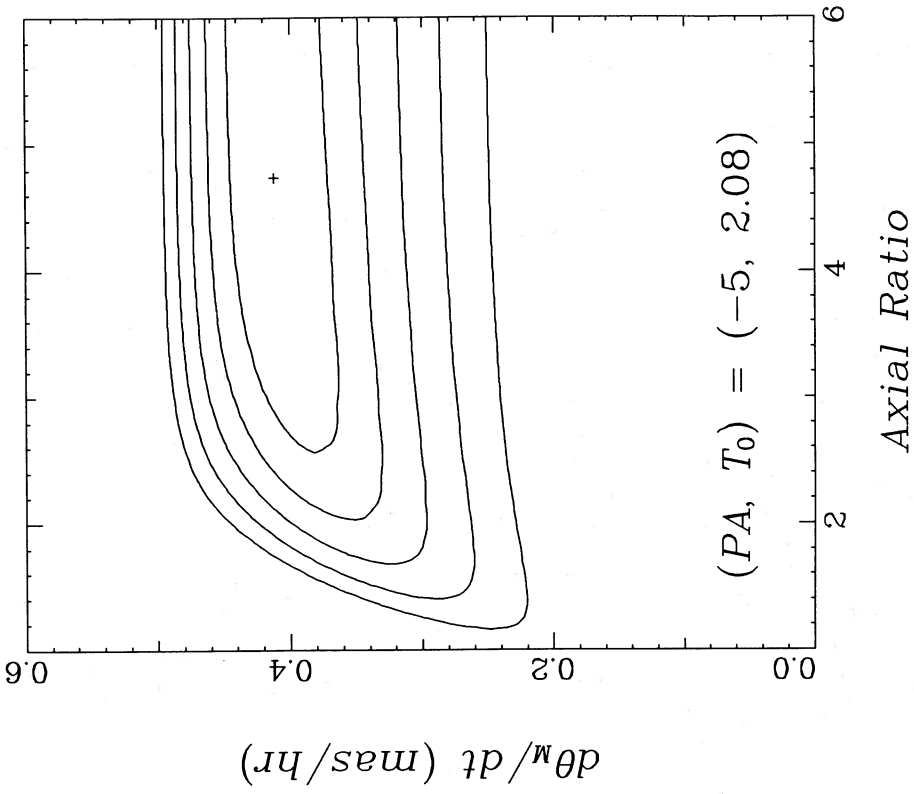


FIG. 10

FIG. 10.—The parameters θ_M vs. A of the expanding elliptical Gaussian model for an extreme set of *a priori* parameter values: $(\lambda, t_0, P) = (-5^\circ, \text{JD } 2,446,102.08, 4.95 \text{ hr})$. A cross marks the best-fit values. Solid curves denote 1 σ through 5 σ error contours.

7.76 with 6 degrees of freedom, which has a fractional probability of 0.26 of being exceeded when the model is correct, which is still a good fit to the data.

With a limited data set, it is worthwhile to identify qualitatively which data points contribute what pieces of information to the final fit. For example, the KY and BY upper limits show the lack of significant structure at small scales. The BY upper limits place an upper limit of 15 mJy on an unresolved (smaller than 0.4 mas) core. The KY upper limits place a lower limit on the FWHM size of the dominant component of ~ 0.7 mas. We fit each day's data to the model separately to further probe which data contained what information and to test the robustness of our model fit. The fit to the February 5 data is very similar to the overall fit. The upper limit on θ_{scat} is less well constrained. There is no information in the February 5 VLBI data about the orientation of the major axis, (which is set by *a priori* information). The fit to the February 8 data alone is marginal statistically, but still results in similar values for the model parameters. The *a priori* flare timing information combines with the size information to determine $\dot{\theta}_M$. The only information lacking here is a lower limit on θ_{scat} , which permits some larger values of $\dot{\theta}_M$. The upper limits on KY/OY at the beginning of February 5, when the intrinsic source size of the model is small, set the lower limits on θ_{scat} in the overall fit.

d) Interpretation

The model fit allows us to draw the following conclusions about the flares observed on February 5 and 8. The times at which flares began follow the radio period suggested in Molnar, Reid, and Grindlay (1984, 1985). As the expansion velocity is not equal to zero (Fig. 9), we can conclude that the data are not consistent with simple, static source structure. As the axial ratio is not unity, the data are not consistent with circularly symmetric structure. As the best-fit parameters have a probable χ^2 , the data are consistent with a source expanding linearly in time from zero size at the flare beginning in at least one dimension. As the axial ratio is not infinite for our best estimate of the position angle, the linear expansion is likely occurring both along the axis of elongation and transverse to it. Finally, the expanding structure is convolved with a fixed-size Gaussian which matches well the effect expected for interstellar scattering computed by extrapolating the results of Wilkinson, Spencer, and Nelson (1987).

It is suggestive to interpret the elongation in terms of a double-sided jet model analogous to that of SS 433. An estimate of the projected bulk velocity, made by taking the proper motion of the model half maximum points measured from the center for a source at 10 kpc (the minimum distance to Cyg X-3 using the *IAU* galactic center distance of 8.5 kpc [Dickey 1983]), is $0.28 \pm 0.03c$, a value strikingly close to the actual bulk velocity of SS 433 (0.26c).

While the expanding elliptical Gaussian model suffices to reveal the qualitative structure in our data set, it has two shortcomings for quantitative parameter estimation within the double-sided jet interpretation. First, the estimation of the projected bulk velocity is systematically affected by the geometry assumed. Second, one cannot directly estimate the intrinsic expansion velocity of the jet components (i.e., expansion transverse to the bulk motion). We therefore fit the data to an alternative model with the same number of free parameters that will allow us to assess the affect of geometry on the projected bulk velocity and to directly estimate the intrinsic expansion velocity. The alternative model consists of an equal double Gaussian, for which the separation between the components and the FWHMs of each component grow linearly with time from flare onset, again convolved with a circular Gaussian scattering disk. As our first model has a centrally condensed brightness distribution, it is likely to overestimate the bulk velocity. In contrast the alternative model assumes no emission arises from a (central) core and so will likely underestimate the bulk velocity. The two results, therefore, should span the range of values that would be obtained for most models.

We specify the alternative model as follows with parameters expressed in such a way as to make the comparison to the earlier results as clear as possible. We define an axial ratio as the ratio of the FWHM of the jet components (presumed to be the same for each) to their separation. As these both expand linearly with time, the axial ratio is a constant

$$A = \dot{\theta}_{\text{sep}} / \dot{\theta}_{\text{FWHM}}, \quad (5)$$

where $\dot{\theta}_{\text{sep}}$ is the angular rate of separation of the two components and $\dot{\theta}_{\text{FWHM}}$ is the angular rate of expansion of the intrinsic FWHM of the components. The observed size of each component as a function of time is given by

$$\theta^2(t) = \theta_{\text{scat}}^2 + [\dot{\theta}_{\text{FWHM}}(t - t_0)]^2. \quad (6)$$

As observed on the sky, the two components are offset in angle toward the east (x) and north (y)

$$x_{1,2} = \pm \frac{1}{2} \dot{\theta}_{\text{sep}}(t - t_0) \sin \chi, \quad (7)$$

$$y_{1,2} = \pm \frac{1}{2} \dot{\theta}_{\text{sep}}(t - t_0) \cos \chi. \quad (8)$$

The correlated flux density is then

$$V(u, v) = S \exp \left[-\frac{\pi^2 \theta^2}{4 \ln 2} (u^2 + v^2) \right] \cos [2\pi(ux_1 + vy_1)]. \quad (9)$$

As before we take $(\chi, t_0, P) = (5^\circ, \text{JD } 2,446,102.05, 4.95 \text{ hr})$ and solve for $\dot{\theta}_{\text{sep}}$, A , and θ_{scat} . The best-fit values are $(0.28 \text{ mas h}^{-1}, 1.50, 0.71 \text{ mas})$. In Figure 11 we plot the best value and 1σ through 5σ contours on the $(A, \dot{\theta}_{\text{sep}})$ plane (again considering θ_{scat} uninteresting and allowing it to vary). Taking θ_{scat} to be the only interesting parameter, its 1σ error is 0.08 mas. The projected bulk velocity is now $0.19 \pm 0.03c$, considerably lower than in the previous model. (This value may also be consistent with a physical bulk velocity of $0.26c$, if either the inclination of the jet axis to the plane of the sky is 43° or the inclination is less but the distance is as great as 14 kpc). By comparing the results for both models, we conclude that the actual projected bulk velocity lies between $0.16c$ and $0.31c$ for a distance of 10 kpc, where both statistical and systematic effects are accounted for. The circular expansion velocity of each jet component is 0.13 ± 0.02 ($\dot{\theta}_{\text{FWHM}} = 0.19 \pm 0.03 \text{ mas h}^{-1}$), in quantitative agreement with our predicted range of $0.05c$ to

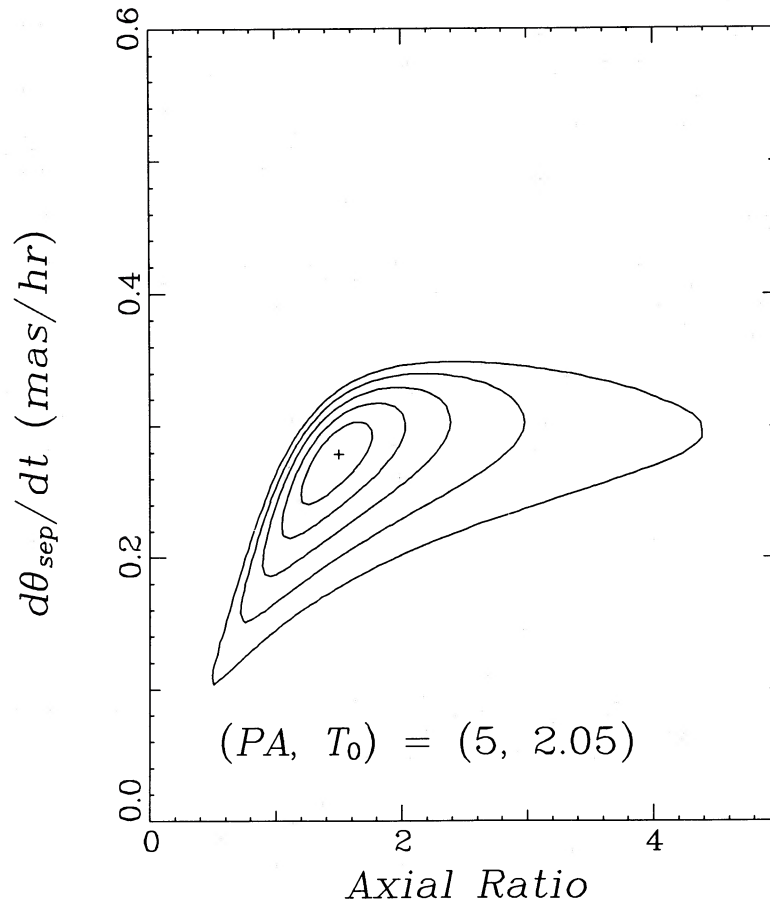


FIG. 11.—The parameters θ_{sep} vs. A of the expanding equal double Gaussian model for the best set of *a priori* parameter values: $(\chi, t_0, P) = (5^\circ, \text{JD } 2,446,102.05, 4.95 \text{ hr})$. A cross marks the best-fit values. Solid curves denote 1σ through 5σ error contours.

$0.25c$ (Molnar, Reid, and Grindlay 1985). Finally we note that the value of θ_{scat} , unlike the value of θ_{sep} , is not significantly different in the alternative model, indicating that it is not sensitive to the chosen geometric details.

In Figure 12 we show contour maps of how an equal double model flare would appear at flare onset, and 1.7, 3.3, and 5.0 hours later. As we did in Figure 8 for the elliptical Gaussian model, we show maps both with and without the interstellar scattering. Comparison of the maps with scattering (i.e., those that represent how the source should appear to us) in Figures 8 and 12 shows how similar the two models are in the first 5 hr of a flare, explaining why both models provide equally good fits to the data.

Previous estimates of the projected bulk velocity of Cyg X-3, which were made during giant radio flares, are consistent with our value. Geldzhaler *et al.* (1983) fitted their data to an elliptical Gaussian model and found an expansion rate of $0.42 \pm 0.08 \text{ mas h}^{-1}$ (cf. $0.40 \pm 0.04 \text{ mas h}^{-1}$ for our elliptical Gaussian fit). Spencer *et al.* (1986) fitted their data to a near-equal double model and found expansion rates between 0.19 and 0.75 mas h^{-1} , depending on the time of onset they use (cf. $0.28 \pm 0.04 \text{ mas h}^{-1}$ for our equal double fit). As both of these data sets were obtained weeks after flare onset, the velocity determinations are limited by the inability to separate the effects of many overlapping flares.

The opening half-angle, β , implied by this model is $\sim 40^\circ$ ($\beta \approx \sin^{-1} 1/A$), rather larger than the $\sim 2^\circ$ estimated for SS 433 (Margon 1981). This may be at the root of several other differences between the two sources. The observable lifetime of a given flare is shorter for Cyg X-3 than for SS 433, as evidenced by the lack of arcsecond structure as well as the shorter time scales seen in the light curve of Cyg X-3 (cf. Johnston *et al.* [1984] for the light curve of SS 433). Since electron lifetimes in synchrotron models are tied to the rate of change in volume, the lack of arcsecond structure and shorter time scales for flux density variation in Cyg X-3 could follow directly from poorer collimation. Katz, Wright, and Lawrence (1984) found no evidence of the Br γ line in the infrared spectrum of Cyg X-3, which one would expect to detect if the jet of Cyg X-3 has the strong thermal emission lines seen in SS 433. The poor collimation implied by our model may broaden such a line enough to preclude detection.

IV. FURTHER WORK

High-frequency VLBI observations of Cyg X-3 offer a rare opportunity to study the structural and spectral evolution of a radio jet in its earliest stages. Observations are facilitated by its relatively high flux density, short time scale of variation, and northerly declination. In particular the time scale of jet evolution in Cyg X-3 (and other X-ray binaries) is much shorter than for jets in active galactic nuclei, and the understanding of the physical conditions in the central engines is more detailed. These factors make Cyg X-3 an important laboratory for detailed theories of relativistic jet formation and evolution.

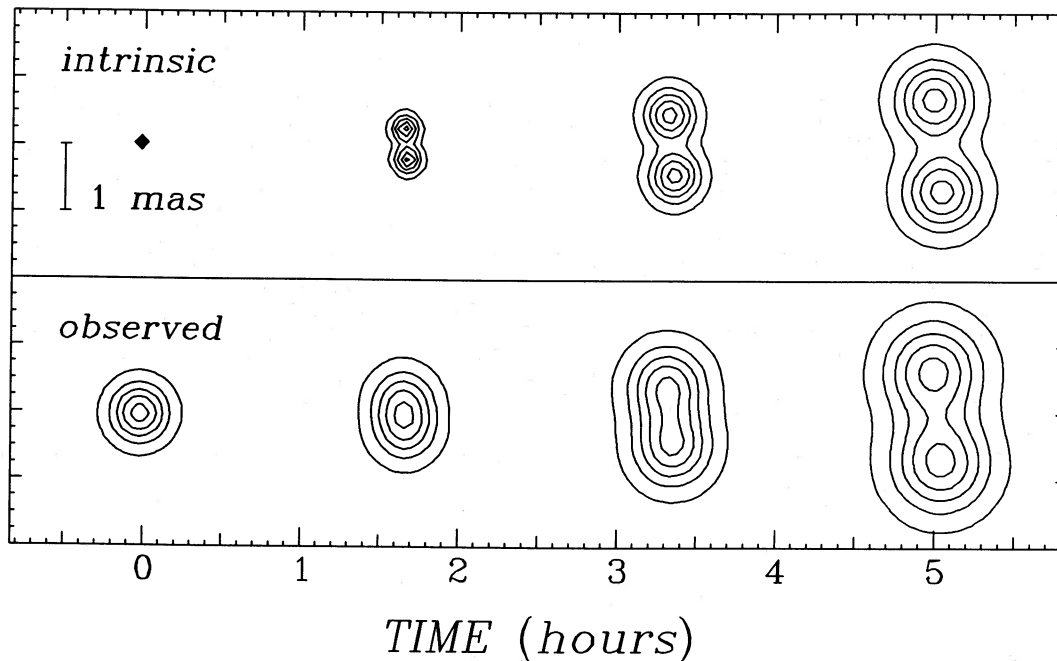


FIG. 12.—Contour maps of an equal double model flare at flare onset, and 1.7, 3.3, and 5.0 hr later, using model parameters determined by the VLBI data. North is up and east to the left. A bar indicates the scale in milliarseconds. The map centers are offset horizontally according to the time they represent (as indicated on the x-axis). The upper row of maps represent the intrinsic source structure, while the lower row represent the observed source structure after inclusion of the effect of interstellar scattering. Contours are at 10%, 30%, 50%, 70%, and 90% of peak brightness.

Further VLBI observations with greater coverage in the (u, v) plane will allow more detailed modeling of the jet structure. Continuous data spanning two or more flares may facilitate more direct measurement of the bulk velocity by observing a position offset between successive flares. Observations of a number of flares at different epochs could show whether the projected bulk velocity or the orientation of the jet vary. (In SS 433, they show a regular precession period.)

We have recently obtained more extensive VLBI observations that will be able to test and extend the results reported here. Even the new data set is limited because scattering restricts analysis to short baselines and none of the crucial short baselines are interconnected (Bonn-Onsala, Green Bank-Haystack, and Owens Valley-VLA). Further advances in detailing source structure will require a greater density of short spacings such as will be afforded by the first three VLBA stations (Pietown, Los Alamos, and Kitt Peak) when combined with Owens Valley, the VLA, and Goldstone. This six-station array will provide 15 baselines with detectable correlated flux density, compared to three in the six-station array used to obtain our new data set. It will also provide 10 closure phases, essential for detection of asymmetry in the source, compared with no closure phases in our new data set. Further advances still will be made possible using the 43 GHz capability of the VLBA, which will increase the effective resolution by a factor of 4 because of the reduced effects of scattering at higher frequencies, and which will increase by a factor of 2 the length of the longest useful baseline, thus increasing the total number of useful baselines.

REFERENCES

- Abell, G. O., and Margon, B. 1979, *Nature*, **279**, 701.
 Anderson, B., Conway, R. G., Davis, R. J., Peckham, R. J., Richards, P. J., Spencer, R. E., and Wilkinson, P. N. 1972, *Nature Phys. Sci.*, **239**, 117.
 Avni, Y. 1976, *Ap. J.*, **210**, 642.
 Avni, Y., Soltan, A., Tananbaum, H., and Zamorani, G. 1980, *Ap. J.*, **238**, 800.
 Avni, Y., and Tananbaum, H. 1986, *Ap. J.*, **305**, 83.
 Crane, P. C. 1984, A Guide to Very-Long-Baseline Interferometry at the Very large Array, NRAO Memorandum.
 Dickey, J. M. 1983, *Ap. J. (Letters)*, **273**, L71.
 Downes, D., and Rinehart, R. 1966, *Ap. J.*, **144**, 937.
 Ferrari, A., Trussoni, E., Rosner, R., and Tsinganos, K. 1985, *Ap. J.*, **294**, 397.
 Geldzahler, B. J., et al. 1983, *Ap. J. (Letters)*, **273**, L65.
 Gregory, P. C., Kronberg, P. P., Seaquist, E. R., Hughes, V. A., Woodsworth, A., Viner, M. R., and Retallack, D. 1972, *Nature*, **239**, 440.
 Gregory, P. C., and Seaquist, E. R. 1974, *Ap. J.*, **194**, 715.
 Hinteregger, H. F., et al. 1972, *Nature Phys. Sci.*, **240**, 159.
 Hjellming, R. M., and Johnston, K. J. 1981a, *Nature*, **290**, 100.
 ———. 1981b, *Ap. J. (Letters)*, **246**, L141.
 Johnston, K. J., et al. 1984, *A.J.*, **89**, 509.
 Katz, J. I., Wright, E. L., and Lawrence, C. R. 1984, *A.J.*, **89**, 1604.
 Kifune, T., Sadzinska, M., Wdowczyk, J., Wolfendale, A. W., Norton, A. J., and Warwick, R. S. 1987, *M.N.R.A.S.*, **228**, 243.
 Margon, B. 1981, *Ann. NY Acad. Sci.*, **357**, 403.
 Molnar, L. A. 1985, Ph.D. thesis, Harvard University.
 ———. 1986, in *Physics of Accretion onto Compact Objects* ed. K. Mason, M. Watson, and N. White (NY: Springer), p. 313.
 Molnar, L. A., and Mauche, C. W. 1986, *Ap. J.*, **310**, 343.
 Molnar, L. A., Reid, M. J., and Grindlay, J. E. 1984, *Nature*, **310**, 662.
 ———. 1985, in *Radio Stars*, ed. R. M. Hjellming and D. M. Gibson (Dordrecht: Reidel), p. 329.
 Spencer, R. E., Swinney, R. W., Johnston, K. J., and Hjellming, R. M. 1986, *Ap. J.*, **309**, 694.
 Wendker, H. J. 1970, *Astr. Ap.*, **4**, 378.
 White, N. E., and Holt, S. S. 1982, *Ap. J.*, **257**, 318.
 Wilkinson, P. N., Spencer, R. E., and Nelson, R. F. 1987, *M.N.R.A.S.*, in press.

J. E. GRINDLAY, L. A. MOLNAR, and M. J. REID: Harvard-Smithsonian Center for Astrophysics, 60 Garden Street, Cambridge, MA 02138